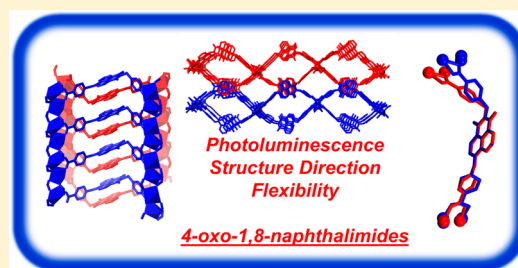


## Flexible Porous Coordination Polymers from Divergent Photoluminescent 4-Oxo-1,8-naphthalimide Ligands

Chris S. Hawes,<sup>\*,†</sup> Kevin Byrne,<sup>‡</sup> Wolfgang Schmitt,<sup>‡</sup> and Thorfinnur Gunnlaugsson<sup>\*,†</sup><sup>†</sup>School of Chemistry and Trinity Biomedical Sciences Institute (TBSI) and <sup>‡</sup>School of Chemistry and Centre for Research on Adaptive Nanostructures and Nanodevices (CRANN), Trinity College Dublin, The University of Dublin, Dublin 2, Ireland

## Supporting Information

**ABSTRACT:** Two new luminescent ditopic naphthalimide-derived ligands, *N*-(4-cyanophenylmethylene)-4-(4-cyanophenoxy)-1,8-naphthalimide (L3) and *N*-(4-carboxyphenylmethylene)-4-(4-carboxyphenoxy)-1,8-naphthalimide (H<sub>2</sub>L4), have been prepared, and their coordination chemistry has been explored in the synthesis of three new coordination polymer materials. Complex poly-[Ag(L3)<sub>2</sub>]BF<sub>4</sub>·4.5H<sub>2</sub>O·0.5THF (1) is a 3-fold 2D → 2D parallel interpenetrated coordination polymer in which three interwoven sheets define inter- and intralayer channels containing anions and solvent molecules. Molecules of L3 interact in 1 through dominant head-to-head  $\pi$ - $\pi$  stacking interactions, in an opposite aggregation mode to that observed in the free ligand in the crystalline phase. Complexes poly-[Cu(L4)(OH<sub>2</sub>)]·2DMF·0.5H<sub>2</sub>O (2) and poly-[Cd<sub>2</sub>(L4)<sub>2</sub>(OH<sub>2</sub>)<sub>2</sub>]·1.5DMF·3H<sub>2</sub>O (3) are related noninterpenetrated two-dimensional coordination polymers defined by one-dimensional metal-carboxylate chains, forming layers that interdigitate with adjacent networks through naphthalimide  $\pi$ - $\pi$  interactions. Both materials undergo structural rearrangements on solvent exchange with acetonitrile; in the case of 3, this transformation can be followed by single-crystal X-ray diffraction, revealing the structure of the acetonitrile solvate poly-[Cd<sub>2</sub>(OH<sub>2</sub>)<sub>2</sub>(L4)<sub>2</sub>]·2MeCN (4), which shows a significant compression of the primary channels to accommodate the solvent guest molecules. Both materials display modest CO<sub>2</sub> adsorption after complete evacuation, and the original expanded phases can be regenerated by reimmersion in DMF. The photophysical properties of each ligand and complex were also explored, which revealed variations in emission wavelength, based on solid-state interactions, including a notable shift in the fluorescence emission band of 3 upon structural rearrangement to 4.



## INTRODUCTION

The study of functional coordination polymer materials has been a consistent highlight in materials chemistry since the first reports of rationally designed extended coordination networks in the early 1990s.<sup>1</sup> Since then, enormous progress has been made in designing and understanding the properties of coordination polymer materials.<sup>2</sup> A particular area of interest is flexible, structurally responsive materials, in which “breathing” processes can take place upon an external stimulus, often involving guest exchange.<sup>3</sup> Such materials have been widely explored for gated adsorption processes and can often display fascinating structural properties.<sup>4</sup> A recent example reported by Kaskel et al. showed the unexpected and rapid desorption of guest molecules following a pressure-dependent structural rearrangement upon guest uptake.<sup>5</sup> In principle, framework flexibility can be employed to enhance the adsorption selectivity for particular analytes, an important consideration for sensing applications where such behavior is coupled with a signaling mechanism.<sup>6</sup> Framework flexibility can be achieved in several ways. Ligands containing flexible backbone groups are often employed, to allow for low-energy structural rearrangements based on alterations of the bridging geometry between metal ions, although this approach can lead to materials that undergo irreversible collapse on evacuation.<sup>7</sup> Flexibility can also be

imparted by other mechanisms, such as reorientation of the metal coordination environment, by reorientation of interpenetrated networks, or by interlayer rearrangements of two-dimensional materials.<sup>8</sup>

The 1,8-naphthalimide skeleton has been widely employed in supramolecular chemistry as a photoactive scaffold that can be readily functionalized with metal binding sites or incorporated into supramolecular architectures.<sup>9</sup> The presence of an electron-donating group in the 3- or 4-position, typically an amine group, provides a green-emitting fluorophore with good photochemical stability and good to excellent quantum yields.<sup>10</sup> Such systems have been used to great effect as fluorescent sensors and probes for ions and biomolecules, as well as in cellular imaging applications,<sup>11</sup> and in the generation of intriguing supramolecular assemblies.<sup>12</sup> Although somewhat more amenable to larger scale syntheses with a broad scope of substitution patterns, relatively fewer studies have reported the properties of 4-oxo-1,8-naphthalimides.<sup>13</sup> The emission properties of these compounds are similar to the amino derivatives, albeit with higher energy of absorption and smaller Stokes shifts, owing to a decrease in the  $\pi$ -donor capabilities of the

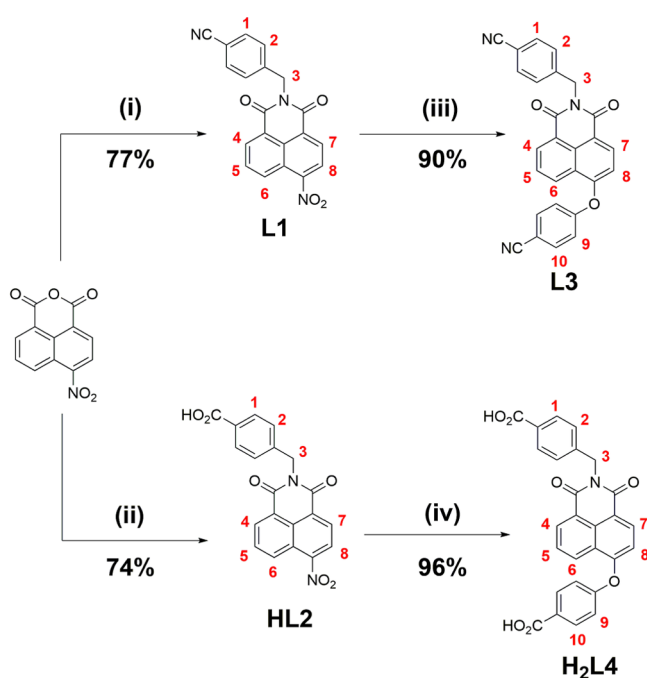
Received: September 4, 2016

alkoxy or phenolic substituents, as recently demonstrated by Thilagar and co-workers.<sup>14</sup> Although the coordination chemistry of many monotopic naphthalimide derivatives has been well studied,<sup>15</sup> few examples are known of naphthalimide ligands containing divergent coordinating groups for the synthesis of photoactive coordination polymer materials. This discrepancy is particularly striking given the wealth of fascinating extended networks that have been reported containing the more synthetically facile 1,4,5,8-naphthalenetetracarboxylic diimide core.<sup>16</sup> Here we report the synthesis of two divergent 4-oxo-1,8-naphthalimide-derived ligands, their photophysical properties, and their use in generating novel luminescent and guest-responsive coordination polymer materials. To the best of our knowledge, these are the first examples of coordination polymers derived from ligands containing the versatile 4-oxo-1,8-naphthalimide core.

## RESULTS AND DISCUSSION

**Synthesis of L3 and H<sub>2</sub>L4 and X-ray Crystal Structure of L3.** The synthesis of the ligands L3 and H<sub>2</sub>L4 is outlined in Scheme 1. The starting materials L1 and HL2 were each

Scheme 1. Synthesis of L1–H<sub>2</sub>L4<sup>a</sup>



<sup>a</sup>Numbering scheme for <sup>1</sup>H NMR shown in red. Reagents and conditions: (i) 4-aminomethylbenzonitrile, HOAc, 120 °C, 6 h; (ii) 4-aminomethylbenzoic acid, HOAc, 120 °C, 6 h; (iii) 4-cyanophenol, K<sub>2</sub>CO<sub>3</sub>, DMSO (Ar), 110 °C, 3 h; (iv) 4-hydroxybenzoic acid, K<sub>2</sub>CO<sub>3</sub>, DMSO (Ar), 120 °C, 3 h.

prepared by condensation of the commercially available 4-nitro-1,8-naphthalic anhydride with the appropriate amine in glacial acetic acid at 120 °C. In both cases, the final products L3 and H<sub>2</sub>L4 were prepared by displacement of the electron-deficient aromatic nitro group by an appropriate phenolate under basic conditions in DMSO solution. The reaction of L1 with 4-cyanophenol in DMSO gave L3 as an off-white powder in an overall 69% yield (two steps), while the reaction of 4-hydroxybenzoic acid with HL2 afforded H<sub>2</sub>L4 in an overall yield of 71% over two steps. The identity and purity of all

organic compounds were confirmed using the standard methods (see full details in the Experimental Section and the Supporting Information).

Single crystals of L3 were prepared by recrystallization from hot ethyl acetate and were analyzed by single-crystal X-ray diffraction. The diffraction data were solved and the structure was refined in the triclinic space group *P* $\bar{1}$ , providing a model containing one complete molecule of L3 in the asymmetric unit with no additional solvent or guest molecules. The two phenyl rings of L3 adopt the expected non-coplanar orientation with respect to the central naphthalimide unit by virtue of rotation about the methylene and oxo spacers, and the resulting *anti* orientation of the terminal nitrile groups leads to a separation between the nitrile nitrogen atoms of 19.085(3) Å. A simple numerical representation of the conformation of L3 can be given by the dihedral angle C5–C8–O3–C21, the rotation of the two *ipso* carbon atoms of the two outer phenyl rings about the vector between the two flexible linking atoms, equal to 120.4(2)°. A slight deformation from planarity is evident in the imide group, leading to a dislocation of 0.31 Å for methylene carbon atom C8 from the naphthalimide mean plane. The structure of L3 is shown in Figure 1.

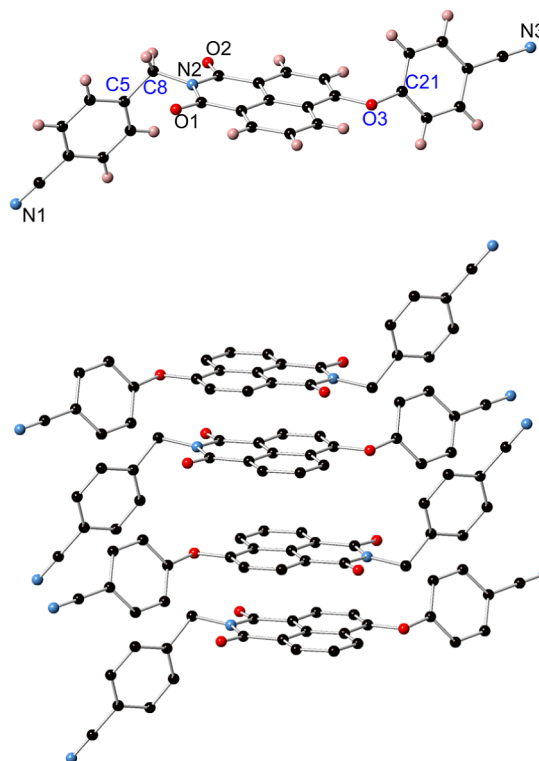


**Figure 1.** (Top) Structure of L3 with partial atom-labeling scheme. The atoms C5–C8–O3–C21 used to define the torsional behavior of the ligand in this and the following structures are labeled in blue. (Bottom) Intermolecular  $\pi$ – $\pi$  interactions between naphthalimide groups in the structure of L3, with hydrogen atoms omitted for clarity.

Intermolecular interactions in the structure of L3 are dominated by parallel offset face-to-face  $\pi$ – $\pi$  interactions, which align the naphthalimide groups into head-to-tail stacks oriented parallel to the crystallographic *b* axis. The minimum interatomic distance for these interactions is 3.560(3) Å (C18–C12), with the mean interplanar distance of 3.35 Å indicative of a strong  $\pi$ – $\pi$  interaction. The two unique cyanophenyl groups

that extend outward from these columns associate into loosely packed layers in the *ab* plane with only minor  $\pi$ - $\pi$  overlap between nearby groups.

**Structure of Poly-[Ag(L3)<sub>2</sub>]BF<sub>4</sub>·4.5H<sub>2</sub>O·0.5THF, 1.** The soft Lewis-basic nature of the donor sites in L3 prompted the use of a compatible metal cation to study the coordination chemistry of the system, and the silver(I) ion was selected based on its lability and affinity for nitrile donor ligands.<sup>17</sup> Crystals of poly-[Ag(L3)<sub>2</sub>]BF<sub>4</sub>·4.5H<sub>2</sub>O·0.5THF (**1**) were prepared by combining solutions of L3 and silver tetrafluoroborate in THF, giving colorless crystals after standing in the dark for 48 h. Analysis by single-crystal X-ray diffraction provided a structure model in the monoclinic space group *C2/c*. The asymmetric unit of complex **1** contains one molecule of L3 and one silver ion occupying a crystallographic special position. Charge balance requirements mandate the presence of half of one tetrafluoroborate anion per asymmetric unit; this anion was poorly localized, but was modeled over two representative positions (Supporting Information). The silver ion within the structure of **1** is coordinated by four nitrile groups from symmetry-related L3 species and adopts a regular tetrahedral geometry with all N–Ag–N angles in the range 102.4(2)–118.21(13)°, as shown in Figure 2. The two unique Ag–N

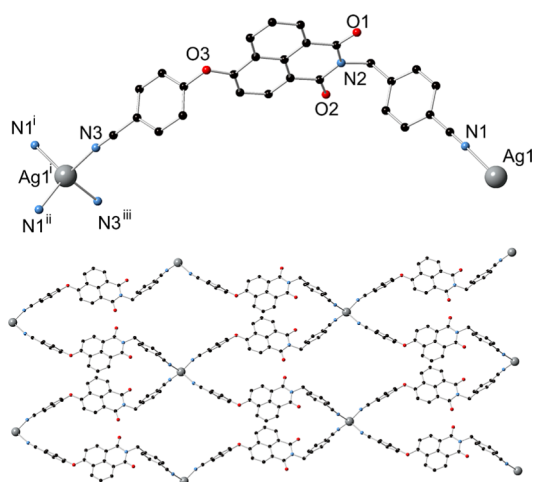


**Figure 2.** (Top) Ligand geometry and coordination environment in the structure of **1**. (Bottom) Extended structure of a single network in **1** viewed perpendicular to the two-dimensional sheet. Hydrogen atoms and anions are omitted for clarity. Symmetry codes used to generate equivalent atoms: (i)  $-x-3/2, y-1/2, +z$ ; (ii)  $x-3/2, y-1/2, +z$ ; (iii)  $-x, +y, 3/2-z$ .

bond lengths of 2.261(4) and 2.241(3) Å for the oxo- and methylene-linked benzonitrile groups, respectively, are within the typically observed values for silver–nitrile interactions from polynitrile donors in coordination polymers.<sup>17</sup> The L3 species adopts a similar orientation of the nitrile groups to that observed in the structure of the free ligand, although with the dihedral angle C5–C8–O3–C21 of 94.7(4)° lessened compared to L3 itself. As a result, the separation between the terminal nitrile nitrogen atoms is contracted to 17.506(5) Å, giving a Ag...Ag distance of 20.7936(16) Å.

The extended structure of **1** comprises a two-dimensional (4,4) network propagated in the *ac* plane, with four-connected silver ions linked by bridging L3 molecules into an undulated layer. Each individual network of **1** contains large windows oriented perpendicular to the direction of propagation, which

are occupied by an additional two interpenetrating networks, providing an uncommon 3-fold 2D → 2D parallel interpenetrated structure, as demonstrated in Figure 3. The

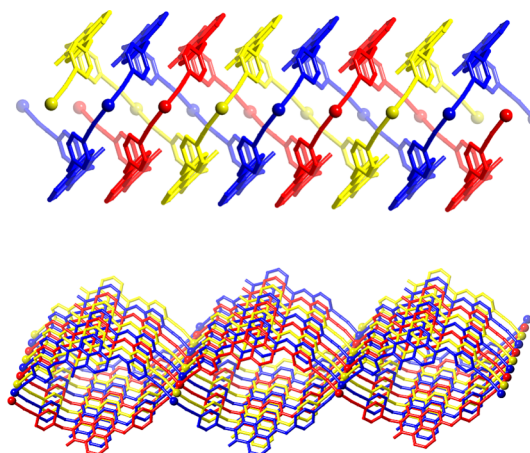


**Figure 3.** Interpenetration mode of complex **1** with independent networks colored separately, showing  $\pi$ - $\pi$  interactions between three interpenetrated networks around a single channel (top) and overall two-dimensional structure of the assembly (bottom).

interwoven networks interact through robust parallel offset face-to-face  $\pi$ - $\pi$  interactions with an unusual head-to-head alignment of adjacent naphthalimide groups enforced by the directionality of the individual networks. The mean interplanar distance of these interactions of 3.34 Å and minimum interatomic distance of 3.282(4) Å (C9–C18) are consistent with the strong  $\pi$ - $\pi$  interactions observed in the structure of the free ligand, albeit with an inverted orientation. Two sets of one-dimensional channels oriented parallel to the *a* axis are present within the extended structure of **1**, within which reside the poorly localized tetrafluoroborate anions, and lattice solvent molecules. The three interwoven networks encapsulate a series of narrow, helical intralayer channels, while the offset stacking of adjacent layers defines slightly larger interlayer channels. The combined volume of the two channels, containing both anions and solvent molecules, accounts for approximately 29% of the unit cell volume, divided approximately 3:2 in favor of the interlayer channels. Microanalysis on an air-dried sample suggested a solvation of 4.5 water molecules and 0.5 THF molecule per [Ag(L3)<sub>2</sub>]BF<sub>4</sub> repeat unit. This assignment is in agreement with thermogravimetric analysis data (Supporting Information), which shows the slow loss of 9.4 wt % below 170 °C (calculated 10.0% for 4.5 H<sub>2</sub>O, 0.5 THF), before the onset of decomposition at approximately 250 °C. The relatively high temperature of desolvation is most likely indicative of pore blocking by the delocalized tetrafluoroborate anions, preventing free exchange of solvent molecules throughout the narrow anion/solvent channels. Attempts to perturb these solvent molecules by soaking in acetonitrile or in 1,4-dioxane led to destruction of the framework, most likely due to the well-known coordinative lability of the Ag<sup>I</sup> ion.

**Structure of Poly-[Cu(L4)(OH<sub>2</sub>)]·2DMF·0.5H<sub>2</sub>O, 2.** In order to explore the coordination chemistry of the carboxylic acid-functionalized ligand H<sub>2</sub>L4, reactions were carried out with divalent d-block metal ions copper(II) and cadmium(II), on the basis of high Lewis acidity of the d<sup>9</sup> species and the lack of interference with ligand fluorescence processes from the d<sup>10</sup> species. The reaction of H<sub>2</sub>L4 with copper nitrate trihydrate in

a 5:95 H<sub>2</sub>O/DMF solvent mixture at 100 °C for 4 h gave light green crystals, which were isolated and analyzed by single-crystal X-ray diffraction. The diffraction data were solved and refined in the triclinic space group  $P\bar{1}$ , with the asymmetric unit containing one molecule of fully deprotonated L4, two unique Cu<sup>II</sup> ions residing on crystallographic special positions, one aqua ligand, and two noncoordinating DMF molecules with slight crystallographic disorder on one site. Both copper ions adopt Jahn–Teller distorted tetragonal coordination geometries, albeit with varying degrees of axial coordination. Copper ion Cu1 is coordinated in the equatorial plane by two carboxylate oxygen atoms and two aqua ligands in a *trans* orientation, with Cu–O distances of 1.939(3) Å for carboxylate and 1.929(3) Å for aqua donors. The axial positions are occupied by weakly interacting carboxylate oxygen atom O2, at a Cu–O distance of 2.836(3) Å. Copper ion Cu2 is coordinated by four carboxylate oxygen atoms in the equatorial plane, at Cu–O distances of 1.955(3) and 1.941(2) Å for O2 and O6, respectively, while the axial positions are involved in a weak interaction with the strongly bound aqua ligand of the adjacent Cu1 site, at a Cu–O separation of 2.499(3) Å. The metal site environment of **2** is shown in Figure 4. The L4

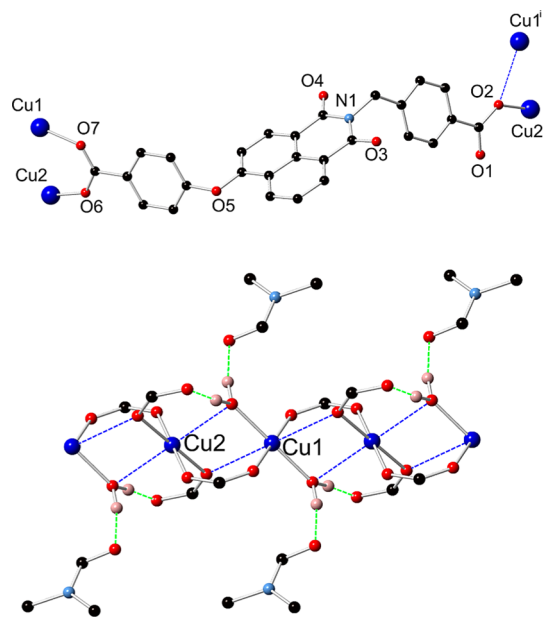


**Figure 4.** Ligand geometry (top) and metal coordination and hydrogen-bonding environment (bottom) in the structure of **2**. Hydrogen bonds are shown as green dashed lines, and long Cu–O interactions along the Jahn–Teller axes are shown as blue dashes. Hydrogen atoms not participating in hydrogen bonding and additional lattice solvent molecules are omitted for clarity. Symmetry codes used to generate equivalent atoms: (i)  $+x, +y, z-1$ .

molecule within the asymmetric unit interacts with four metal sites through a bridging carboxylate functionality. The carboxylate group of the oxo-benzoate arm coordinates in a  $\mu_2\text{-}\kappa\text{O}:\kappa\text{O}'$  mode to Cu1 and Cu2, while the other carboxylate group bridges two metal ions through the same oxygen atom, coordinating to an equatorial position of the Cu2 coordination sphere and weakly interacting at the axial position of the Cu1 site. The noncoordinating carboxylate oxygen atom from this group participates in a hydrogen-bonding interaction with the aqua ligand, with a donor–acceptor distance of O8...O1 2.560(4) Å and D–H...A angle of 173(7)°. The ligand

molecule adopts a similar conformation to that of L2 in complex **1**, with a dihedral angle C5–C8–O5–C21 of 97.3(4)°, Figure 4.

The extended structure of **2** is defined by one-dimensional columns of carboxylate- and aqua-bridged Cu<sup>II</sup> ions oriented parallel to the *a* axis, which are linked in the *c* direction by L4 ligands. The resulting two-dimensional layer contains one-dimensional intralayer channels parallel to *a* and bordered by the naphthalimide groups of L4, which are oriented approximately perpendicular to the channel axis. One of the two unique lattice DMF molecules is localized within these channels, displaying slight rotational disorder. Unlike the case of complex **1**, in which similar layers undergo parallel 2D → 2D interpenetration through  $\pi$ – $\pi$  interactions, adjacent layers in complex **2** associate in the *c* direction, without interpenetration but instead through interdigitation of the naphthalimide groups. The resulting  $\pi$ – $\pi$  interactions, with 180° head-to-tail geometry, are parallel with mean interplanar distances of 3.32 and 3.30 Å and minimum interatomic distances of 3.383(6) Å (C10–C16) and 3.468(6) Å (C18–C14), respectively, for the two unique interactions. As well as the intralayer channels, linkage of adjacent networks through naphthalimide  $\pi$ – $\pi$  interactions leaves additional interlayer solvent channels parallel to the *a* axis and bordered by the metal–carboxylate chains. Within these channels, a well-resolved DMF molecule is observed; this molecule participates in a hydrogen-bonding interaction with the aqua ligand, at a D...A distance of 2.625(4) Å and D–H...A angle of 170(6)° for O8–H8D...O9. These channels are rhombic in shape, with approximate interatomic dimensions of 9 × 9 Å, compared to the slit-shaped intralayer channels, in which the DMF molecules occupy bound volumes of dimensions of ca. 5 × 10 Å, as shown in Figure 5.

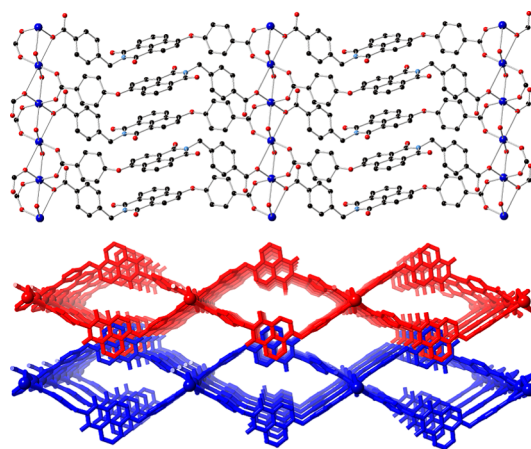


**Figure 5.** Extended structure of **2**, showing the connectivity of a single layer (top) and interdigitation of two adjacent layers, with independent networks colored separately (bottom). Hydrogen atoms and lattice solvent molecules are omitted for clarity.

Microanalysis suggested the presence of an additional water molecule per two copper sites, presumably facilitated by the disordered orientation of the intralayer DMF molecule and providing a formula for the bulk material of poly-[Cu(L4)(OH<sub>2</sub>)]·2DMF·0.5H<sub>2</sub>O. Thermogravimetric analysis of **2** revealed a two-step mass loss of 21.2% within the range of 30–250 °C, consistent with the loss of the noncoordinating solvent molecules (calculated 22%), with the onset of decomposition above 300 °C.

**Structure of Poly-[Cd<sub>2</sub>(OH)<sub>2</sub>(L4)<sub>2</sub>·1.5DMF·H<sub>2</sub>O, 3.** The reaction of H<sub>2</sub>L4 with cadmium nitrate in a 5:95 H<sub>2</sub>O/DMF solvent mixture gave colorless rod crystals after 24 h at 100 °C, which were analyzed by single-crystal X-ray diffraction, and from which a structure model was generated in the orthorhombic space group *Pccn*. The asymmetric unit of **3** contains one molecule of L4, fully deprotonated, and two unique cadmium ions. Both cadmium ions adopt six-coordinate, distorted octahedral coordination geometries, and both occupy crystallographic special positions. Cadmium ion Cd1 is coordinated by two equivalent chelating carboxylate groups, which bridge Cd1 and Cd2 in a  $\mu_2\text{-}\kappa\text{O},\text{O}':\kappa\text{O}$  coordination mode, and the remaining two *cis*-oriented coordination sites are occupied by carboxylate oxygen atoms from a bridging  $\mu_2\text{-}\kappa\text{O}:\kappa\text{O}'$ -disposed carboxylate group, as shown in Figure 6.

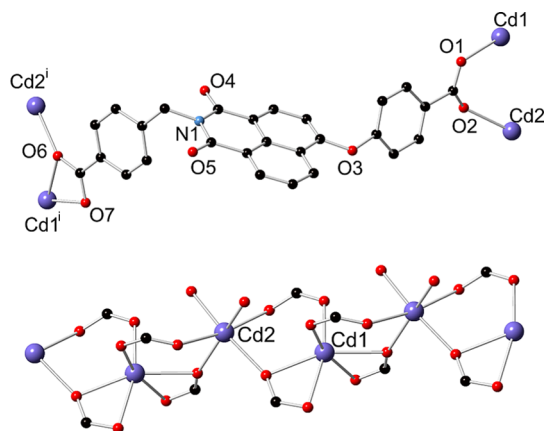


**Figure 6.** Ligand environment (top) and metal coordination environment (bottom) in the structure of **3** with partial heteroatom labeling scheme. Hydrogen atoms and lattice solvent molecules are omitted for clarity. Symmetry codes used to generate equivalent atoms: (i)  $x-1/2, 2-y, 3/2-z$ .

Cadmium ion Cd2 is coordinated by four monodentate carboxylate oxygen atoms, each of which undergoes the previously described bridging mode, and two *cis*-oriented oxygen atoms from aqua ligands. Each L4 molecule coordinates to four cadmium ions, and the torsion angle C5–C8–O3–C21 of 90.4(11)° compares closely to that observed in the other complexes. Each of the seven unique Cd–O distances fall in the range 2.222(10)–2.362(7) Å, and both ions display moderate distortion from ideal octahedral geometry ( $\Sigma = 153^\circ$  and  $73^\circ$  for Cd1 and Cd2, respectively),<sup>18</sup> with a smaller value for Cd2 consistent with the entirely monodentate coordination sphere.

The extended structure of **3** is a two-dimensional sheet consisting of one-dimensional cadmium–carboxylate chains oriented parallel to the crystallographic *b* axis, which are linked in the *a* direction by the bridging L4 groups. Similarly to the case of **2**, one-dimensional channels remain both within the sheets and between adjacent layers, as shown in Figure 7. The intralayer channels are of a comparable size and shape to those in **2**, containing cavities of approximately  $5 \times 10$  Å and bounded in the *b* direction by the intruding edges of the perpendicular-oriented naphthalimide rings. The interlayer channels are also of comparable dimensions to those observed in **2**, being approximately square with minimum interatomic distances of ca.  $9 \times 9$  Å. Although the contents of the interlayer channels could not be crystallographically modeled, the intralayer channels contain well-resolved DMF molecules

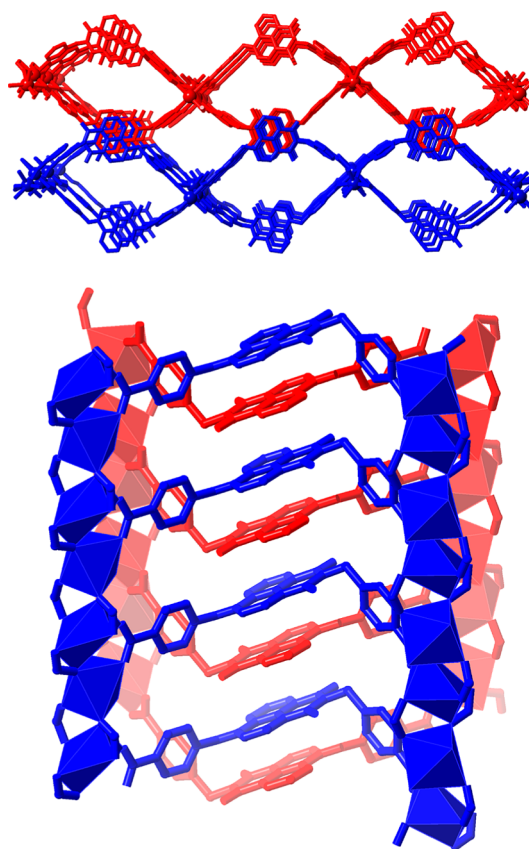


**Figure 7.** Extended structure of **3** showing the interdigitation between two adjacent layers, viewed parallel (top) and perpendicular (bottom) to the one-dimensional solvent channels, with independent networks colored separately. Hydrogen atoms and lattice solvent molecules are omitted for clarity.

modeled at half-occupancy, which lie nearly flat along the long axis of the rhombic channels. Reminiscent of the extended structure of **2**, adjacent layers in the structure of **3** associate through head-to-tail interdigitation of the naphthalimide groups (Figure 7), forming strong parallel face-to-face  $\pi$ – $\pi$  interactions at a mean interplanar distances of 3.37 and 3.38 Å for the two unique interactions. Microanalysis revealed a formula for the air-dried sample of 0.75 DMF molecule and 1.5 water molecules per cadmium ion, although thermogravimetric analysis of a freshly isolated sample shows a total mass loss of 16% between 30 and 160 °C with onset at room temperature (calculated 12.5%), consistent with partial desolvation occurring upon standing in ambient conditions.

**Solvent Exchange Studies and Structure of Poly-[Cd<sub>2</sub>(OH)<sub>2</sub>(L4)<sub>2</sub>·2MeCN, 4.** The presence of contiguous solvent-accessible volumes in both **2** and **3** prompted an investigation into the guest exchange properties of each compound. Acetonitrile was chosen as the exchange solvent, as a relatively volatile guest that can readily exchange with lattice DMF and water molecules, but is unlikely to disrupt the coordination sites leading to collapse of the structure. In the case of compound **2**, acetonitrile exchange efficiently removed all lattice solvent molecules, confirmed by thermogravimetric analysis (TGA), and provided a material that could be readily desolvated at 100 °C. X-ray powder diffraction showed that although the exchanged material was crystalline, a transition to another crystalline phase had taken place (Supporting Information). Despite our efforts, we were unable to effect

Table 1. Summary of Crystal and Refinement Parameters for All Compounds

identification code	L3	1	2	3	4
empirical formula	C <sub>27</sub> H <sub>15</sub> N <sub>3</sub> O <sub>3</sub>	C <sub>54</sub> H <sub>30</sub> AgBF <sub>4</sub> N <sub>6</sub> O <sub>6</sub>	C <sub>33</sub> H <sub>31</sub> CuN <sub>3</sub> O <sub>10</sub>	C <sub>57</sub> H <sub>37</sub> Cd <sub>2</sub> N <sub>3</sub> O <sub>17</sub>	C <sub>29</sub> H <sub>18</sub> CdN <sub>2</sub> O <sub>8</sub>
fw	429.42	1053.52	693.15	1260.69	634.85
temp/K	100(2)	100(2)	100(2)	100(2)	100(2)
cryst syst	monoclinic	monoclinic	triclinic	orthorhombic	orthorhombic
space group	<i>P</i> 2 <sub>1</sub> / <i>c</i>	<i>C</i> 2/ <i>c</i>	<i>P</i> $\bar{1}$	<i>Pccn</i>	<i>Pccn</i>
<i>a</i> /Å	10.4422(10)	4.4466(4)	6.8306(9)	37.4447(10)	40.5139(15)
<i>b</i> /Å	6.8590(7)	39.390(3)	10.7920(13)	7.3470(2)	7.2658(3)
<i>c</i> /Å	29.249(3)	31.168(2)	20.523(3)	23.1978(6)	18.5724(8)
$\alpha$ /deg	90	90	88.621(3)	90	90
$\beta$ /deg	95.909(2)	90.755(2)	88.801(3)	90	90
$\gamma$ /deg	90	90	80.851(3)	90	90
volume/Å <sup>3</sup>	2083.8(4)	5458.7(8)	1492.9(3)	6381.9(3)	5467.1(4)
<i>Z</i>	4	4	2	4	8
$\rho_{\text{calc}}$ /cm <sup>3</sup>	1.369	1.282	1.542	1.312	1.543
$\mu$ /mm <sup>-1</sup>	0.091	0.434	0.799	0.73	0.852
<i>F</i> (000)	888	2128	718	2528	2544
cryst size/mm <sup>3</sup>	0.37 × 0.11 × 0.05	0.28 × 0.1 × 0.05	0.08 × 0.05 × 0.05	0.23 × 0.21 × 0.08	0.23 × 0.06 × 0.05
radiation	Mo <i>K</i> $\alpha$ ( $\lambda$ = 0.71073)	Mo <i>K</i> $\alpha$ ( $\lambda$ = 0.71073)	Mo <i>K</i> $\alpha$ ( $\lambda$ = 0.71073)	Mo <i>K</i> $\alpha$ ( $\lambda$ = 0.71073)	Mo <i>K</i> $\alpha$ ( $\lambda$ = 0.71073)
2 $\theta$ range for data collection/deg	3.922 to 54.972	2.446 to 53	3.824 to 52.17	3.512 to 50.998	4.022 to 52
index ranges	-13 ≤ <i>h</i> ≤ 10, -8 ≤ <i>k</i> ≤ 8, -37 ≤ <i>l</i> ≤ 37	-5 ≤ <i>h</i> ≤ 5, -46 ≤ <i>k</i> ≤ 48, -39 ≤ <i>l</i> ≤ 35	-8 ≤ <i>h</i> ≤ 8, -13 ≤ <i>k</i> ≤ 9, -25 ≤ <i>l</i> ≤ 25	-45 ≤ <i>h</i> ≤ 29, -8 ≤ <i>k</i> ≤ 5, -28 ≤ <i>l</i> ≤ 28	-46 ≤ <i>h</i> ≤ 49, -8 ≤ <i>k</i> ≤ 8, -22 ≤ <i>l</i> ≤ 22
reflins collected	37 208	29 855	21 338	51 379	33 987
indep reflins	4762 [ <i>R</i> <sub>int</sub> = 0.0989, <i>R</i> <sub>sigma</sub> = 0.0633]	5684 [ <i>R</i> <sub>int</sub> = 0.0820, <i>R</i> <sub>sigma</sub> = 0.0742]	5934 [ <i>R</i> <sub>int</sub> = 0.0995, <i>R</i> <sub>sigma</sub> = 0.1133]	5936 [ <i>R</i> <sub>int</sub> = 0.0813, <i>R</i> <sub>sigma</sub> = 0.0440]	5366 [ <i>R</i> <sub>int</sub> = 0.1080, <i>R</i> <sub>sigma</sub> = 0.0911]
data/restraints/params	4762/0/298	5684/135/393	5934/16/462	5936/139/382	5366/70/418
goodness-of-fit on <i>F</i> <sup>2</sup>	1.005	1.078	0.982	1.075	1.023
final <i>R</i> indexes [ <i>I</i> ≥ 2 $\sigma$ ( <i>I</i> )]	<i>R</i> <sub>1</sub> = 0.0515, <i>wR</i> <sub>2</sub> = 0.1001	<i>R</i> <sub>1</sub> = 0.0764, <i>wR</i> <sub>2</sub> = 0.2132	<i>R</i> <sub>1</sub> = 0.0516, <i>wR</i> <sub>2</sub> = 0.1037	<i>R</i> <sub>1</sub> = 0.1183, <i>wR</i> <sub>2</sub> = 0.3186	<i>R</i> <sub>1</sub> = 0.0891, <i>wR</i> <sub>2</sub> = 0.1929
final <i>R</i> indexes [all data]	<i>R</i> <sub>1</sub> = 0.1169, <i>wR</i> <sub>2</sub> = 0.1203	<i>R</i> <sub>1</sub> = 0.1148, <i>wR</i> <sub>2</sub> = 0.2352	<i>R</i> <sub>1</sub> = 0.1177, <i>wR</i> <sub>2</sub> = 0.1229	<i>R</i> <sub>1</sub> = 0.1553, <i>wR</i> <sub>2</sub> = 0.3496	<i>R</i> <sub>1</sub> = 0.1847, <i>wR</i> <sub>2</sub> = 0.2357
largest diff peak/hole/e Å <sup>-3</sup>	0.21/-0.28	1.00/-0.69	0.62/-0.63	4.51/-3.14	0.77/-1.30

this transformation on crystals of sufficient quality for single-crystal X-ray diffraction analysis. The equivalent treatment of compound 3 with acetonitrile produced similar results; exchange of the labile lattice DMF molecules from the solvent channels was observed by TGA, while X-ray powder diffraction analysis of the exchanged material showed a new crystalline phase. However, in contrast to 2, this phase was formed with sufficient retention of crystallinity to allow structure determination by single-crystal X-ray diffraction, although with significant disorder in the vicinity of the metal sites.

The X-ray diffraction data for 4 were solved and refined in the orthorhombic space group *Pccn*, equivalent to 3. The unit cell volume of 4 is contracted by ca. 15% from 3, mostly manifested by a contraction of *c* from 23.1978(6) Å to 18.5724(8) Å, with a smaller concurrent increase in *a* from 37.4447(10) Å to 40.5139(15) Å, as summarized in Table 1. The asymmetric unit of 4 contains one molecule of L4, coordinating in an equivalent bridging mode to that in 3 to two unique cadmium sites, although with crystallographic disorder necessitating the splitting of cadmium ion Cd2 into two symmetry-related half-occupancy locations on either side of the previously occupied special position. The torsion angle C5–C8–O5–C21 of 114.9(10)°, compared to 90.4(11)°, is indicative of a conformational change in the L4 environment and an overall flattening of the molecule, which is primarily manifested by a rotation of the imide-bound carboxyphenyl

group, as shown in Figure 8. Notably, whereas compound 3 contained well-localized lattice DMF molecules within the intralayer channels, compound 4 contains one acetonitrile molecule at full occupancy per L4 group. The coordinating aqua ligands and lattice solvent from the interlayer channels in 4 displayed substantial disorder, related to the disorder present on the metal sites themselves, and as a result, the noncoordinating solvent molecules from these channels could not be crystallographically resolved.

The effect of the solvent exchange and framework contraction in 4 is clear when the extended structure is considered. The two-dimensional layers in the *ab* plane are substantially contracted in thickness along *c* when compared to compound 3, with reduction in the size of both the intra- and interlayer solvent channels. This observation is consistent with replacement of the comparatively sterically encumbering DMF molecules in the intralayer channels with the more compact acetonitrile guests, which can be more effectively encapsulated by the contracted naphthalimide walls in 4. Although the  $\pi$ – $\pi$  stacking interactions between sheets are retained in 4, with definite head-to-tail arrangement of the naphthalimide groups, slight variations are present in the mean (naphthyl–naphthyl) interplanar distances (3.434(7) and 3.384(5) Å, compared to 3.372(7) and 3.384(10) Å for 3) and the distance between adjacent naphthyl centroids in each interaction (3.572(5) and 4.173(6) Å for 4 and 3.589(6) and 4.308(7) Å for 3).

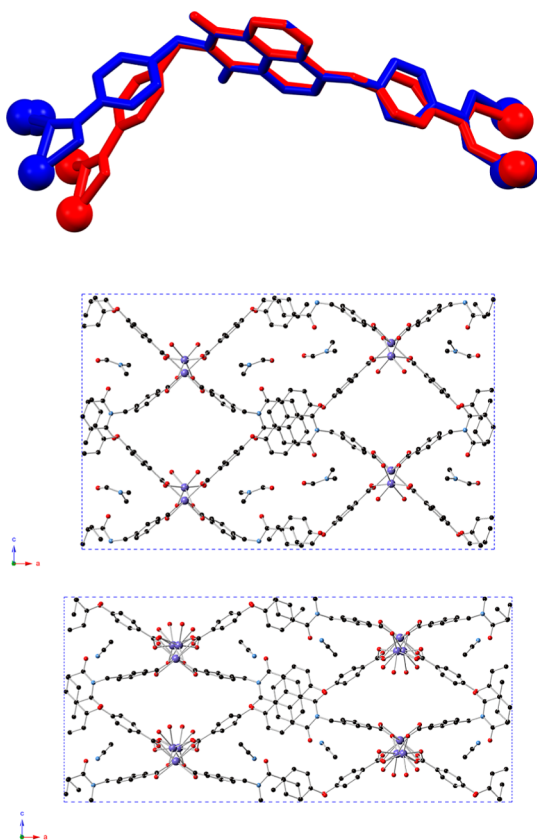


**Figure 8.** Comparison of the structures of 3 and 4. (Top) Ligand conformation in 3 (red) and 4 (blue), overlaid using the rigid naphthalimide groups as anchor points. (Bottom) To-scale comparison of the unit cells of 3 (top) and 4 (bottom), viewed along the [010] vector, with *a* horizontal and *c* vertical. Hydrogen atoms and oxo-benzoate ring torsional disorder are omitted for clarity.

**Gas Adsorption Studies.** Both compounds 2 and 3/4 were examined for their gas uptake properties. In both cases, the noncoordinating lattice solvents were exchanged by soaking the materials in acetonitrile for 48 h (in the process, necessarily converting compound 3 to compound 4), followed by evacuation at 100 °C overnight under dynamic vacuum. Due to the very narrow and polar pore environments in both samples, it was envisaged that CO<sub>2</sub> would be the most appropriate probe gas, where low-temperature N<sub>2</sub> uptake is typically very low for ultramicroporous materials.<sup>19</sup> Indeed, no meaningful 77 K N<sub>2</sub> or H<sub>2</sub> physisorption could be measured for compound 3 or 4 in the micropore-filling pressure range, with any adsorption taking place at or below the instrumental detection limit. However, both compounds displayed moderate CO<sub>2</sub> adsorption in the pressure range 0–1 bar, albeit with slow kinetics particularly in the low-pressure region, accompanied by hysteresis on the desorption branch indicative of a slow desorption process. The CO<sub>2</sub> adsorption isotherms for 2 and 4 are shown in Figure 9.

Compound 2 displayed a maximum uptake of 27 cc(STP)/g at 1 bar, equivalent to 5 wt %, or ca. 0.66 CO<sub>2</sub> molecule per [Cu(L)(OH<sub>2</sub>)] unit. This loading is approximately 1/3 of the observed loading (mol/mol) of DMF guests within the as-synthesized material, consistent with substantial contraction of the framework on evacuation. Measuring an X-ray powder diffraction pattern on the material after the adsorption experiment showed some degree of crystallinity is retained in

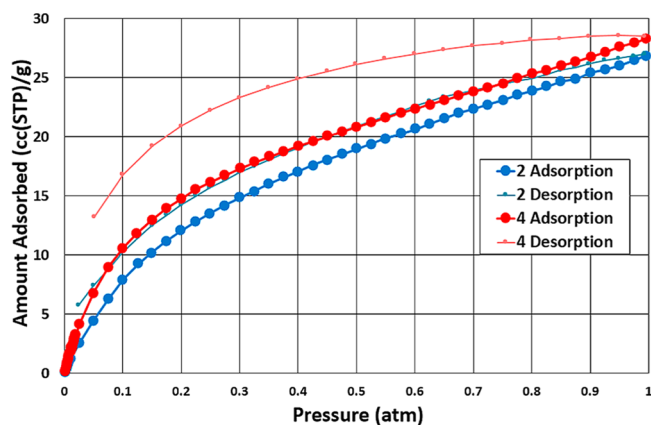


**Figure 9.** CO<sub>2</sub> adsorption isotherms for compounds 2 and 4, measured at 273 K after soaking in acetonitrile and activation under dynamic vacuum at 373 K overnight.

the material after adsorption, though not resembling the original phase or the acetonitrile-exchanged material, suggesting a further structural change takes place upon complete evacuation.

Compound 4 displayed a similar maximum uptake to compound 2, of 29 cc(STP)/g at 1 bar (5.4 wt %). The higher density of the cadmium-containing framework, however, means this value correlates to a marginally higher per-mole CO<sub>2</sub> loading of 0.85 molecule of CO<sub>2</sub> per [Cd(L4)(OH<sub>2</sub>)] repeat unit, which approaches the loading of (crystallographically resolved) lattice acetonitrile in 4. Similar to the case of 2, X-ray powder diffraction of compound 4 after gas adsorption experiments showed that the material retained some degree of crystallinity, although with variation in peak positions consistent with an additional structural rearrangement. In both cases, however, the solvent-exchanged and evacuated materials could be reimmersed in DMF to regenerate the original DMF-solvated phases, as evidenced by X-ray powder diffraction (Supporting Information).

**Photophysical Studies.** Each compound L1–H<sub>2</sub>L4 was examined for its UV–visible absorbance and emission response, and the results are summarized in Table 2. All four

**Table 2.** Summary of Solution-State Photophysical Properties of Compounds L1–H<sub>2</sub>L4

compound	solvent	$\lambda_{\text{abs}}$ (nm)	$\epsilon$ (L·mol <sup>-1</sup> · cm <sup>-1</sup> )	$\lambda_{\text{em}}$ (nm, $\lambda_{\text{ex}}$ = 366 nm)	$\Phi$
L1	CHCl <sub>3</sub>	351	10 200 ± 300		
HL2	DMSO	354	11 100 ± 300		
L3	CHCl <sub>3</sub>	359	14 300 ± 500	420	0.89 ± 0.05
H <sub>2</sub> L4	DMSO	361	15 400 ± 600	440	~0.02

naphthalimide compounds displayed broad absorption bands with  $\lambda_{\text{max}}$  in the range 350–360 nm, and no variations in peak shape or maxima position were observed in the concentration range of 10<sup>-4</sup>–10<sup>-6</sup> M. The 4-nitro-substituted precursors L1 and HL2 exhibited no meaningful fluorescence upon excitation, compared to the 4-oxonaphthalimides L3 and H<sub>2</sub>L4, both of which possess well-defined emission bands in the blue region (Figure 10). Upon excitation at 366 nm in CHCl<sub>3</sub>, compound L3 displayed an emission band with  $\lambda_{\text{max}} = 420$  nm, with partially resolved shoulders in both the absorption and

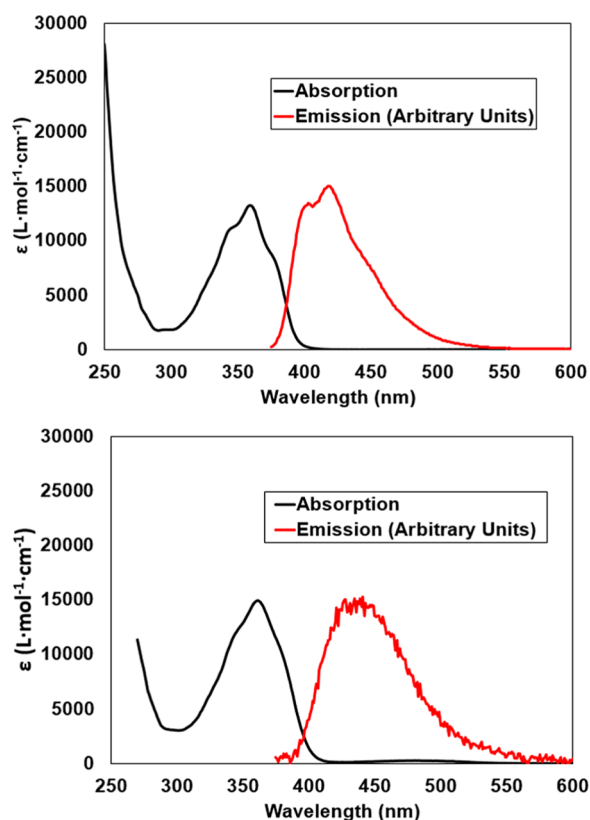


**Figure 10.** UV–visible absorption (black) and emission (red,  $\lambda_{\text{ex}} = 366$  nm) spectra of **L3** (top) and **H<sub>2</sub>L4** (bottom), recorded in  $\text{CHCl}_3$  (40  $\mu\text{M}$ ) and DMSO (75  $\mu\text{M}$ ), respectively.

emission bands. In the solid state, this emission was observed at  $\lambda_{\text{max}} = 480$  nm, with a bathochromic shift following molecular aggregation in the crystalline state. Compound **L3** displayed a relatively high fluorescence quantum yield of  $89\% \pm 5\%$  in solution, using quinine sulfate ( $\Phi_{\text{F}} = 54.6\%$ ,  $\lambda_{\text{ex}} = 366$  nm) in 2 M  $\text{H}_2\text{SO}_4$  as a reference standard.<sup>20</sup> The dicarboxylic acid species **H<sub>2</sub>L4** in DMSO solution displayed an emission maximum at  $\lambda_{\text{max}} = 440$  nm ( $\lambda_{\text{ex}} = 366$  nm), undergoing a less substantial bathochromic shift to 470 nm in the solid state. The fluorescence quantum yield of **H<sub>2</sub>L4** in DMSO solution was measured at ca. 2%.

These quantum yield values can be considered a continuation of the solution-state trend observed for the 4-aryloxo-*N*-ethylnaphthalimides reported by Thilagar et al.<sup>21</sup> In that study, the presence of flexible groups or groups capable of strongly contributing to nonradiative decay attached to the phenolic 4-position caused a reduction in fluorescence quantum yield from 96% for the most rigid and symmetric phenol derivative to <10% for the nitro, thioacetyl, and carboxyaldehyde derivatives. The contributions of carboxylic acid groups to nonradiative decay pathways are well known<sup>22</sup> and most likely lead to the reduction in fluorescence quantum yield in the case of **H<sub>2</sub>L4**.

The fluorescence properties of complexes 1–4 were also characterized in the solid state, as shown in Figure 11. Complex **1** displayed a broad emission band with  $\lambda_{\text{max}} = 455$  nm, a notable hypsochromic shift compared to the free ligand in the solid state. As well as the expected differences in the local polarity of the fluorophore in the free ligand compared to complex **1**, this variation may be rationalized by the differences in the naphthalimide aggregation modes between the free ligand and the complex in the crystalline state. The ligand

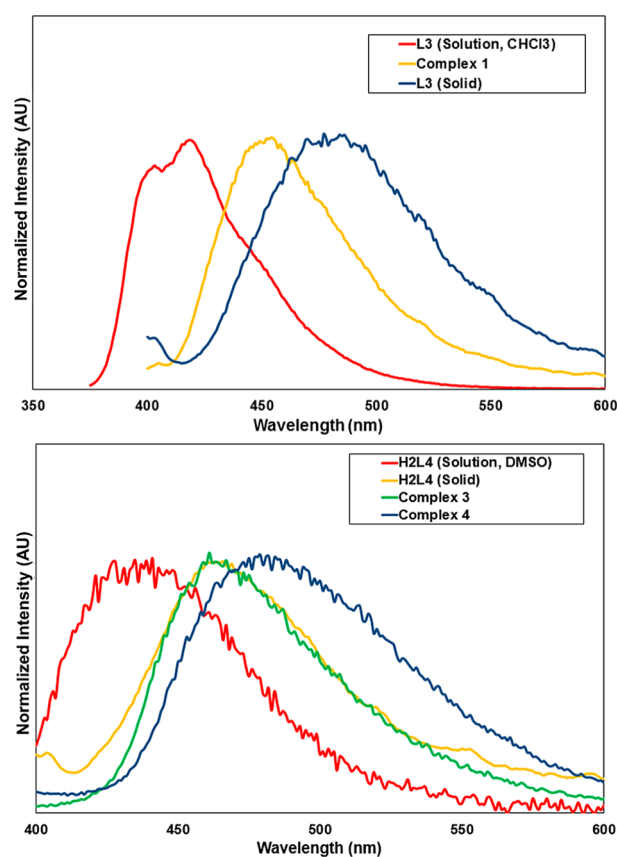


**Figure 11.** Solid-state emission spectra ( $\lambda_{\text{ex}} = 366$  nm) for complex **1** (top) and complexes 3/4 (bottom), compared to their respective free ligands in solution and in the solid state.

adopts a head-to-tail stacking mode for the naphthalimide groups in the crystal structure of the free ligand, while a head-to-head, H-aggregate-type packing mode is adopted in complex **1**. Unsurprisingly, complex **2** displayed no measurable photoluminescence, presumably due to quenching of the naphthalimide excited state by the  $d^9$   $\text{Cu}^{\text{II}}$  ions within the structure.<sup>23</sup> Complex **3** exhibits an emission band effectively superimposable with that of the free ligand in the solid state, with  $\lambda_{\text{max}} = 465$  nm. Interestingly, complex **4**, which differs from complex **3** only by a slight reorientation of the naphthalimide stacks and a change in the size, polarity, and volatility of the encapsulated guest molecules, displays a notably different emission signature. A bathochromic shift in the emission band is observed, with  $\lambda_{\text{max}} = 480$  nm, and is accompanied by a peak broadening, from  $\text{fwhm} = 70$  nm for **3** to 90 nm for **4**.

## DISCUSSION

Comparing the structures of **L3** and complexes 1–4, the flexible linkers are seen to exhibit a relatively narrow range of geometries, where the torsion angle from each aryl group about the vector between the two  $\text{sp}^3$  linkers varies in the range  $90$ – $120^\circ$ . Most likely, the orientation of these freely rotatable groups is dictated by crystal-packing influences more than any preferred position for the low-energy bond rotations involved. More significant in terms of structure direction in the solid state are the dominant face-to-face  $\pi$ – $\pi$  interactions between the naphthalimide groups in each structure. The importance of such interactions in influencing the extended solid-state structure of coordination compounds is well established,<sup>24</sup>

and in this case the interactions between the strongly polarized aromatic surfaces are likely responsible for the resilience of the three-dimensional structures of **2** and **3/4** to solvent exchange, evacuation, and resolution. The low gas loadings and slow desorption kinetics, implied by the apparent hysteresis on the desorption branches of both CO<sub>2</sub> isotherms, are indicative of a very narrow pore environment within both samples after evacuation, which suggests a further contraction of the pores on evacuation. Given the observed pore contraction in **3** to enclose the smaller acetonitrile guest molecule in **4**, a further contraction following evacuation of the material is not unexpected.

The variation in emission behavior in the solid state between complexes **1**, **3**, and **4** and their free ligands **L3** and **H<sub>2</sub>L4** was consistent with the expected behavior, based largely on changes in the solid-state aggregation mode. As the ligand design provides central fluorophores, which are electronically isolated from the metal binding groups, little impact on the emission properties was observed as a direct consequence of metal coordination, evidenced in the case of **H<sub>2</sub>L4** compared with complex **3** in the solid state. The variation in emission properties between complexes **3** and **4** is particularly interesting, as it provides the basis of a fluorescent signaling mechanism for a coupled change in both the local polarity of the fluorophore unit and a structural rearrangement of the host framework without requiring any chemical change to the framework atoms themselves.

## CONCLUSIONS

We have prepared three new coordination polymers, **1**, **2**, and **3**, from the novel luminescent naphthalimide-derived linkers **L3** and **H<sub>2</sub>L4**. In each case, substantial  $\pi$ - $\pi$  interactions dominate the extended structures, leading to dense 3-fold interpenetration in the silver coordination network poly-[Ag(**L3**)<sub>2</sub>]BF<sub>4</sub>·4.5H<sub>2</sub>O·0.5THF (**1**) and a robust and flexible interlayer interaction in the related two-dimensional networks poly-[Cu(**L4**)(OH<sub>2</sub>)]<sub>2</sub>·2DMF·0.5H<sub>2</sub>O (**2**) and poly-[Cd<sub>2</sub>(**L4**)<sub>2</sub>(OH<sub>2</sub>)<sub>2</sub>]<sub>2</sub>·1.5DMF·3H<sub>2</sub>O (**3**). Both compounds **2** and **3** undergo structural rearrangements on solvent exchange; in the case of **3**, this transition can be monitored with single-crystal X-ray diffraction, using which we elucidated the structure of the acetonitrile solvate poly-[Cd<sub>2</sub>(**L4**)<sub>2</sub>(OH<sub>2</sub>)<sub>2</sub>]<sub>2</sub>·2MeCN (**4**). Moreover, CO<sub>2</sub> adsorption experiments showed that both activated materials retained modest guest uptake capacity on complete evacuation, and both materials could be reverted to their original phases by reimmersion in DMF after evacuation. Furthermore, the photophysical properties of the complexes and their parent ligands have been studied, which relate the aggregation mode of the fluorophores in the crystalline state to the photoluminescent properties of the resulting materials. This relationship can be exploited as a means of signaling a structural transformation, as in the case of the transition from **3** to **4** on solvent exchange. These results highlight the usefulness of electronically isolated organic fluorophores in flexible coordination polymer assemblies as reporting elements for chemical sensor devices, and this area of research is currently being pursued in our laboratory.

## EXPERIMENTAL SECTION

**Materials and Methods.** All reagents, solvents, and starting materials were purchased from Sigma-Aldrich, Merck, or Fisher Scientific, were of reagent grade or better, and were used as received. Mass spectra were acquired using a Micromass time-of-flight mass

spectrometer (tof), interfaced to a Waters 2690 HPLC. The instrument was operated in positive or negative mode as required. Leucine enkephalin was used as an internal lock mass. Masses were recorded over the range 100–1000 *m/z*. Elemental analyses were carried out at the Microanalytical Laboratory, School of Chemistry and Chemical Biology, University College Dublin. NMR data were recorded in commercially available deuterated solvents on an Agilent 400-MR spectrometer operating at 400 MHz for <sup>1</sup>H NMR and 100 MHz for <sup>13</sup>C NMR. Chemical shifts are expressed in parts per million (ppm/ $\delta$ ) and were referenced relative to the internal solvent signals. Infrared spectra were recorded on a PerkinElmer Spectrum 100 FTIR spectrometer with universal ATR sampling accessory, in the range 4000–650 cm<sup>-1</sup>. X-ray powder diffraction patterns were collected using a Bruker D2 Phaser instrument with Cu K $\alpha$  radiation ( $\lambda$  = 1.5418 Å). Samples were ground and mounted on silicon sample holders, and data were collected in the  $2\theta$  range 5–55° at room temperature while rotating  $\varphi$  at a speed of 1 rpm. Sample background due to fluorescence was subtracted, and the patterns were compared with those simulated from the single-crystal data collected at 100 K. UV–visible absorption spectra were measured using spectroscopic grade solvents (Sigma-Aldrich) in the range 250–800 nm (CHCl<sub>3</sub>) or 270–800 nm (DMSO) on a Varian Cary 50 Bio spectrophotometer. Fluorescence spectra were measured on a Varian Cary Eclipse fluorimeter. Quantum yields were calculated by comparison with quinine sulfate in 2 M H<sub>2</sub>SO<sub>4</sub> with excitation at 366 nm using an excitation slit width of 2.5 nm for all samples, and emission was integrated across the range 380–600 nm. Solid-state emission spectra were measured at room temperature with powdered samples pressed into films between quartz plates. Gas adsorption isotherms were measured using a Quantachrome Autosorb IQ gas sorption analyzer. Chemically pure (CP) grade He, N<sub>2</sub>, H<sub>2</sub>, and CO<sub>2</sub> gases from BOC gases were used for the measurements.

**X-ray Crystallography.** Structural and refinement parameters are presented in Table 1. All diffraction data were collected using a Bruker APEX-II Duo dual-source instrument using graphite-monochromated Mo K $\alpha$  ( $\lambda$  = 0.710 73 Å) radiation. Data sets were collected using  $\omega$  and  $\varphi$  scans with the samples immersed in oil and maintained at a constant temperature of 100 K using a Cobra cryostream. The data were reduced and processed using the Bruker APEX suite of programs.<sup>25</sup> Multiscan absorption corrections were applied using SADABS.<sup>26</sup> The diffraction data were solved using SHELXT and refined by full-matrix least-squares procedures using SHELXL-2015 within the OLEX-2 GUI.<sup>27–29</sup> The functions minimized were  $\sum w(F_o^2 - F_c^2)$ , with  $w = [\sigma^2(F_o^2) + aP^2 + bP]^{-1}$ , where  $P = [\max(F_o)^2 + 2F_c^2]/3$ . All non-hydrogen atoms were refined with anisotropic displacement parameters. All carbon-bound hydrogen atoms were placed in calculated positions and refined with a riding model, with isotropic displacement parameters equal to either 1.2 or 1.5 times the isotropic equivalent of their carrier atoms. Where appropriate, the positions of hydrogen atoms involved in hydrogen-bonding interactions were refined to provide the best fit for the residual Fourier peaks and assigned a  $U_{iso}$  value equal to 1.5 times that of the nearest associated atom, with the appreciation that the exact positions of these atoms cannot be meaningfully inferred from X-ray diffraction data. The data sets for **1**, **3**, and **4** contained regions of diffuse electron density consistent with totally delocalized lattice solvent molecules, alongside regions of ordered or partially ordered solvents; the scattering contribution from only the diffuse electron density regions to the measured structure factors was accounted for with the SQUEEZE routine to allow for more representative refinement statistics for the framework atoms,<sup>30</sup> and the solvent channel contents were ascertained using TGA and elemental analysis. The reported crystallographic formulas, densities, and  $F_{000}$  values are based on the crystallographically localized atoms only. Particular refinement strategies for each structure, including the specific use of restraints, are provided in the refine\_special\_details sections of the combined crystallographic information file. CCDC 1497724–1497728.

**Synthesis.** *N*-(4-Cyanophenylmethylene)-4-nitro-1,8-naphthalimide, **L1**. 4-Nitro-1,8-naphthalic anhydride (300 mg, 1.2 mmol) and 4-aminomethylbenzotrile (200 mg, 1.5 mmol) were combined in 5

mL of glacial acetic acid. The mixture was heated at 120 °C for 6 h and cooled to room temperature. A 5 mL amount of water was added to the solution, causing the precipitation of an orange powder, which was collected by filtration. The solids were washed with water and methanol and dried in air. Yield: 330 mg (77%). Mp: 243–245 °C. Anal. Found: C, 66.96; H, 2.95; N, 11.65. Calcd for  $C_{20}H_{11}N_3O_4$ : 67.23; H, 3.10; N, 11.76.  $^1H$  NMR  $\delta_H$  (400 MHz,  $CDCl_3$ ): 5.42 (s, 2H,  $H^3$ ), 7.64 (second-order multiplet, 4H,  $H^1 + H^2$ ), 8.02 (dd, 1H,  $^3J_1 = 8.7$  Hz,  $^3J_2 = 7.4$  Hz,  $H^5$ ), 8.42 (d, 1H,  $^3J = 7.9$  Hz,  $H^7$ ), 8.72 (d, 1H,  $^3J = 7.9$  Hz,  $H^8$ ), 8.77 (d, 1H,  $^3J = 7.4$  Hz,  $H^4$ ), 8.86 (d, 1H,  $^3J = 8.8$  Hz,  $H^6$ ).  $^{13}C$  NMR  $\delta_C$  (100 MHz,  $CDCl_3$ ): 43.55, 111.75, 118.57, 122.61, 123.73, 123.88, 126.50, 129.13, 129.67, 129.79, 130.01, 130.28, 132.40, 132.89, 141.65, 149.87, 162.46, 163.26. MS  $m/z$  (APCI) 357.0749  $[M]^-$ , calcd for  $C_{20}H_{11}N_3O_4$  357.0755. IR  $\nu_{max}$  (ATR,  $cm^{-1}$ ): 3073m, 2231s, 1700s, 1660s, 1622m, 1583m sh, 1521s sh, 1461w, 1431m, 1410m, 1378m, 1336s sh, 1309m, 1228s, 1170m, 1024w, 969m, 932w, 862w, 817m sh, 787s, 761s, 713w, 663m, 631m. UV  $\lambda_{max}$  ( $CHCl_3$ ): 351 nm ( $10\,200 \pm 300$  L·mol $^{-1}$ ·cm $^{-1}$ ).

**N-(4-Carboxyphenylmethylene)-4-nitro-1,8-naphthalimide, HL2.** 4-Nitro-1,8-naphthalic anhydride (400 mg, 1.6 mmol) was slurried in 7 mL of glacial acetic acid. To this mixture was added 4-amino-methylbenzoic acid (300 mg, 2.0 mmol), and the mixture was heated at 120 °C for 6 h. The mixture was cooled to room temperature and filtered, and the resulting tan solid was washed with water, methanol, and diethyl ether and dried in air. Yield: 458 mg (74%). Mp: >300 °C. Anal. Found: C, 63.66; H, 3.05; N, 7.29. Calcd for  $C_{20}H_{12}N_2O_6$ : C, 63.83; H, 3.21; N, 7.44.  $^1H$  NMR  $\delta_H$  (400 MHz,  $d_6$ -DMSO): 5.30 (s, 2H,  $H^3$ ), 7.48 (d, 2H,  $^3J = 8.3$  Hz,  $H^2$ ), 7.86 (d, 2H,  $^3J = 8.3$  Hz,  $H^1$ ), 8.08 (dd, 1H,  $^3J_1 = 8.7$  Hz,  $^3J_2 = 7.5$  Hz,  $H^5$ ), 8.53 (d, 1H,  $^3J = 7.8$  Hz,  $H^7$ ), 8.60–8.64 (m, 2H,  $H^4 + H^8$ ), 8.7 (d, 1H,  $^3J = 8.7$  Hz,  $H^6$ ).  $^{13}C$  NMR  $\delta_C$  (100 MHz,  $d_6$ -DMSO): 43.17, 122.66, 122.79, 124.23, 126.52, 127.47, 128.56, 129.02, 129.40, 129.61, 129.92, 130.13, 131.97, 141.87, 149.34, 162.33, 163.10, 167.03. MS  $m/z$  (HR-ESMS): found 375.0617  $[M - H]^-$ , calcd for  $C_{20}H_{11}N_2O_6$  375.0617. IR  $\nu_{max}$  (ATR,  $cm^{-1}$ ): 3078w, 2968w, 2819w, 2653w, 2541w br, 1687s, 1665s, 1611m sh, 1581m sh, 1523s, 1430m, 1380w, 1338s, 1317m, 1296s, 1230s, 1182m, 1099m, 1020w, 965m, 932m, 864m sh, 825m, 784s, 759s, 704m. UV  $\lambda_{max}$  (DMSO): 354 nm ( $11\,100 \pm 300$  L·mol $^{-1}$ ·cm $^{-1}$ ).

**N-(4-Cyanophenylmethylene)-4-(4-cyanophenoxy)-1,8-naphthalimide, L3.** N-(4-Cyanophenylmethylene)-4-nitro-1,8-naphthalimide (L1) (200 mg, 0.56 mmol), 4-cyanophenol (133 mg, 1.1 mmol), and potassium carbonate (240 mg, 1.7 mmol) were combined in 5 mL of anhydrous DMSO. The mixture was heated at 110 °C under argon for 3 h. The mixture was cooled to room temperature, and 20 mL of water was added, causing precipitation of an orange solid. The solids were collected by filtration, washed with 100 mL of water, 50 mL of methanol, and 50 mL of diethyl ether, and dried in air. Yield: 216 mg (90%). Single crystals were prepared by recrystallization from ethyl acetate. Mp: 247–248 °C. Anal. Found: C, 75.31; H, 3.44; N, 9.72. Calcd for  $C_{27}H_{15}N_3O_3$ : C, 75.52; H, 3.52; N, 9.79.  $^1H$  NMR  $\delta_H$  (400 MHz,  $d_6$ -DMSO): 5.33 (s, 2H,  $H^3$ ), 7.32 (d, 1H,  $^3J = 8.3$  Hz,  $H^8$ ), 7.42 (d, 2H,  $^3J = 8.6$  Hz,  $H^9$ ), 7.55 (d, 2H,  $^3J = 8.3$  Hz,  $H^2$ ), 7.78 (d, 2H,  $^3J = 8.4$  Hz,  $H^1$ ), 7.94 (dd, 1H,  $^3J_1 = 8.5$  Hz,  $^3J_2 = 7.3$  Hz,  $H^5$ ), 7.99 (d, 2H,  $^3J = 8.5$  Hz,  $H^{10}$ ), 8.49 (d, 1H,  $^3J = 8.2$  Hz,  $H^7$ ), 8.57–8.62 (m, 2H, overlapping,  $H^4 + H^6$ ).  $^{13}C$  NMR  $\delta_C$  (100 MHz,  $d_6$ -DMSO): 42.85, 107.42, 109.83, 114.26, 117.77, 118.41, 118.76, 120.35, 122.25, 123.93, 127.68, 128.18, 128.37, 129.31, 131.92, 132.35, 132.78, 135.07, 143.08, 157.00, 159.21, 162.88, 163.52. MS  $m/z$  (APCI): 327.0771  $[M - C_6H_4CN]^-$ , calcd for  $C_{20}H_{11}N_2O_3$  327.0770. IR  $\nu_{max}$  (ATR,  $cm^{-1}$ ): 3070w br, 2227s, 1692s, 1655s, 1581s, 1495s, 1465m, 1404w, 1381m, 1340s sh, 1305w, 1234s sh, 1170m, 1109w, 1071w, 1023w, 984m, 943m, 834m, 781s, 758m, 662m. UV  $\lambda_{max}$  ( $CHCl_3$ ): 359 nm ( $14\,300 \pm 500$  L·mol $^{-1}$ ·cm $^{-1}$ ). Phase purity was confirmed by X-ray powder diffraction (Supporting Information).

**N-(4-Carboxyphenylmethylene)-4-(4-carboxyphenoxy)-1,8-naphthalimide, H<sub>2</sub>L4.** N-(4-Carboxyphenylmethylene)-4-nitro-1,8-naphthalimide (HL2) (200 mg, 0.53 mmol), 4-hydroxybenzoic acid (147 mg, 1.1 mmol), and potassium carbonate (440 mg, 3 mmol) were combined in 5 mL of anhydrous DMSO. The mixture was heated at 120 °C under an argon atmosphere for 3 h and cooled to room

temperature. A 20 mL amount of water was added, to give a dark green solution, which was acidified with dilute acetic acid, causing precipitation of a tan solid. The solid was filtered, washed with 3 mL of DMSO, 100 mL of water, 100 mL of methanol, and 50 mL of diethyl ether, and dried in air. Yield: 237 mg (96%). Mp: >300 °C. Anal. Found: C, 67.51; H, 3.50; N, 2.90. Calcd for  $C_{27}H_{17}NO_7 \cdot 0.66H_2O$ : C, 67.64; H, 3.86; N, 2.92.  $^1H$  NMR  $\delta_H$  (400 MHz,  $d_6$ -DMSO): 5.31 (s, 2H,  $H^3$ ), 7.22 (d, 1H,  $^3J = 8.2$  Hz,  $H^8$ ), 7.34 (d, 2H,  $^3J = 8.9$  Hz,  $H^9$ ), 7.46 (d, 2H,  $^3J = 8.3$  Hz,  $H^2$ ), 7.88 (d, 2H,  $^3J = 8.3$  Hz,  $H^1$ ), 7.93 (dd, 1H,  $^3J_1 = 8.3$  Hz,  $^3J_2 = 7.5$  Hz,  $H^5$ ), 8.07 (d, 2H,  $^3J = 8.8$  Hz,  $H^{10}$ ), 8.48 (d, 1H,  $^3J = 8.2$  Hz,  $H^7$ ), 8.60 (d, 1H,  $^3J = 7.4$  Hz,  $H^4$ ), 8.64 (d, 1H,  $^3J = 8.5$  Hz,  $H^6$ ).  $^{13}C$  NMR  $\delta_C$  (100 MHz,  $d_6$ -DMSO): 42.82, 113.26, 117.11, 119.65, 122.16, 123.79, 127.36, 127.51, 128.45, 129.22, 129.46, 129.71, 131.89, 131.96, 132.92, 142.30, 157.85, 158.71, 162.87, 163.52, 166.61, 167.10. MS  $m/z$  (HR-ESMS): 466.0916  $[M - H]^-$ , calcd for  $C_{27}H_{16}NO_7$  466.0927; 232.5413  $[M - 2H]^{2-}$ , calcd for  $C_{27}H_{15}NO_7^{2-}$  232.5430. IR  $\nu_{max}$  (ATR,  $cm^{-1}$ ): 2992w br, 2657w, 2546w, 1680s sh, 1651s, 1579s sh, 1504m, 1468w, 1424m, 1384s, 1346m, 1317w, 1292m, 1234s sh, 1213m, 1168m, 1126m, 1100m, 1017w, 939w, 874m, 780s, 754s, 704m. UV  $\lambda_{max}$  (DMSO): 361 nm ( $15\,400 \pm 600$  L·mol $^{-1}$ ·cm $^{-1}$ ).

**Poly-[Ag(L3)]<sub>2</sub>BF<sub>4</sub>·4.5H<sub>2</sub>O·0.5THF, 1.** Compound L3 (20 mg, 47  $\mu$ mol) was suspended in 1 mL of THF with the aid of brief sonication. To this mixture was added a solution of silver tetrafluoroborate (8 mg, 41  $\mu$ mol) in 2 mL of THF, and the mixture was capped and sealed in foil and allowed to stand for 2 days. After this period, colorless crystals of the product were isolated by filtration, washed with THF, and dried in air. Yield: 13 mg (47%). Mp: 169–172 °C (dec). Anal. Found: C, 57.42; H, 3.09; N, 6.73. Calcd for  $[Ag(L3)]_2BF_4 \cdot 0.5THF \cdot 4.5H_2O$ ,  $C_{56}H_{43}N_6O_{11}BF_4Ag$ : C, 57.45; H, 3.70; N, 7.18. IR  $\nu_{max}$  (ATR,  $cm^{-1}$ ): 3420w br, 3071w, 2954w, 2872w, 2248s, 1696s, 1650s sh, 1624w, 1578s sh, 1498s, 1466m, 1402m, 1382s, 1350s, 1303m sh, 1232s sh, 1180m, 1132w, 1109w, 1053s sh, 987m, 942m, 883m, 846m, 813m, 780s, 757m, 665m. Phase purity was confirmed by X-ray powder diffraction (Supporting Information).

**Poly-[Cu(L4)(OH)<sub>2</sub>]<sub>2</sub>·2DMF·0.5H<sub>2</sub>O, 2.** Compound H<sub>2</sub>L4 (20 mg, 42  $\mu$ mol) and copper nitrate trihydrate (24 mg, 99  $\mu$ mol) were combined in 2 mL of a mixture of 5% H<sub>2</sub>O in DMF. The mixture was briefly sonicated, capped, and heated to 100 °C. After 4 h, the mixture was sonicated for 5 s to separate the product from a small quantity of copper oxide particles, and the green solids were decanted and isolated by filtration. The solids were washed with several portions of DMF and dried in air. Yield: 13 mg (44%). Mp: >300 °C. Anal. Found: C, 56.39; H, 4.26; N, 5.66. Calcd for  $[Cu(L4)(OH)_2]_2 \cdot 2DMF \cdot 0.5H_2O$ ,  $C_{33}H_{32}N_3O_{10.5}Cu$ : C, 56.45; H, 4.59; N, 5.98. IR  $\nu_{max}$  (ATR,  $cm^{-1}$ ): 2870w, 2802m br, 1698m, 1654s sh, 1591s sh, 1545m, 1502m, 1467w, 1436w, 1380s, 1347s, 1233m sh, 1209m, 1184m, 1164w, 1134w, 1092w sh, 1019m, 991m, 948m, 884m, 787s, 767s, 711m sh. Phase purity was confirmed by X-ray powder diffraction (Supporting Information).

**Poly-[Cd<sub>2</sub>(L4)<sub>2</sub>(OH)<sub>2</sub>]<sub>2</sub>·1.5DMF·3H<sub>2</sub>O, 3.** Compound H<sub>2</sub>L4 (10 mg; 21  $\mu$ mol) and cadmium nitrate tetrahydrate (12 mg; 39  $\mu$ mol) were added to 1 mL of a 5% H<sub>2</sub>O in DMF mixture and sealed in a screw-cap vial. The mixture was briefly sonicated before being heated to 100 °C and left to dwell at this temperature for 24 h. After this period, the mixture was filtered hot, and the pale yellow crystals were washed with DMF and dried in air. Yield: 6 mg (43%). Mp: >300 °C. Anal. Found: C, 53.36; H, 3.13; N, 3.74. Calcd for  $[Cd_2(L4)_2(OH)_2]_2 \cdot 1.5DMF \cdot 3H_2O$ ,  $C_{58.5}H_{46.5}N_{3.5}O_{18.5}Cd_2$ : C, 53.26; H, 3.55; N, 3.72. IR  $\nu_{max}$  (ATR,  $cm^{-1}$ ): 3300 w br, 1700m, 1654s sh, 1593s sh, 1518m, 1507m sh, 1398m, 1379s, 1345m, 1256m, 1234s, 1209m, 1173m, 1131m, 1107m, 1078m, 1016w, 997m, 960w, 946m, 887m, 804w, 791w, 778m, 754m, 710m, 672m. Phase purity was confirmed by X-ray powder diffraction (Supporting Information).

**Conversion of Poly-[Cd<sub>2</sub>(L4)<sub>2</sub>(OH)<sub>2</sub>]<sub>2</sub>·1.5DMF·3H<sub>2</sub>O, 3, to Poly-[Cd<sub>2</sub>(L4)<sub>2</sub>(OH)<sub>2</sub>]<sub>2</sub>·2MeCN, 4.** A sample of solid 3 (20 mg) was suspended in 20 mL of acetonitrile with vigorous mixing. The mixture was allowed to stand for 48 h, with the solvent decanted and replaced with fresh acetonitrile, with mixing, every 12 h. The exchanged material was recovered by filtration in quantitative yield. The lattice

solvent is lost almost immediately on standing in air, and so the solvation of the bulk material is estimated based on the crystallographically located solvent molecules only. Mp: >300 °C. IR  $\nu_{\max}$  (ATR,  $\text{cm}^{-1}$ ): 3257 w br, 2359m, 2342m sh, 1702m sh, 1655s sh, 1592m, 1579m, 1559m, 1518m, 1500s, 1399s, 1383s, 1346s, 1259s, 1235s, 1209m, 1173m, 1132w, 1105w, 1069w, 1017m, 995m, 945m, 861m, 804m, 779s, 755m, 669m. Phase purity was confirmed by X-ray powder diffraction (Supporting Information).

## ■ ASSOCIATED CONTENT

### 📄 Supporting Information

The Supporting Information is available free of charge on the ACS Publications website at DOI: 10.1021/acs.inorgchem.6b02137.

Additional X-ray crystallography figures, thermogravimetric analysis data, X-ray powder diffraction patterns, NMR spectra for all compounds, and additional photophysical characterization data (PDF)  
Crystallographic data (CIF)

## ■ AUTHOR INFORMATION

### Corresponding Authors

\*E-mail (C. S. Hawes): [hawescs@tcd.ie](mailto:hawescs@tcd.ie).

\*E-mail (T. Gunnlaugsson): [gunnlaut@tcd.ie](mailto:gunnlaut@tcd.ie).

### Author Contributions

The manuscript was written through contributions of all authors. All authors have given approval to the final version of the manuscript.

### Notes

The authors declare no competing financial interest.

## ■ ACKNOWLEDGMENTS

The authors gratefully acknowledge the Irish Research Council (IRC) (Postdoctoral Fellowship GOIPD/2015/446 to C.S.H.), Science Foundation Ireland (SFI) for SFI PI Awards (10/IN.1/B2999 and 13/IA/1865 to T.G., 13/IA/1896 to W.S.), TCD Dean of Research Pathfinder Award (T.G. and C.S.H.), the European Research Council (ERC; CoG 2014-647719 to W.S.), and TCD School of Chemistry for financial support.

## ■ REFERENCES

- (1) Hoskins, B. F.; Robson, R. Design and construction of a new class of scaffolding-like materials comprising infinite polymeric frameworks of 3D-linked molecular rods. A reappraisal of the zinc cyanide and cadmium cyanide structures and the synthesis and structure of the diamond-related frameworks  $[\text{N}(\text{CH}_3)_4][\text{CuIzNII}(\text{CN})_4]$  and  $\text{CuI}[4,4',4'',4''']\text{-tetracyanotetraphenylmethane}]\text{BF}_4 \cdot \text{x} \cdot \text{C}_6\text{H}_5\text{NO}_2$ . *J. Am. Chem. Soc.* **1990**, *112*, 1546–1554. Batten, S. R.; Hoskins, B. F.; Robson, R. 2,4,6-Tri(4-pyridyl)-1,3,5-triazine as a 3-Connecting Building Block for Infinite Nets. *Angew. Chem., Int. Ed. Engl.* **1995**, *34*, 820–822.
- (2) Cui, Y.; Li, B.; He, H.; Zhou, W.; Chen, B.; Qian, G. Metal–Organic Frameworks as Platforms for Functional Materials. *Acc. Chem. Res.* **2016**, *49*, 483–493. Furukawa, H.; Cordova, K. E.; O’Keeffe, M.; Yaghi, O. M. The Chemistry and Applications of Metal–Organic Frameworks. *Science* **2013**, *341*, 123044. Farruseng, D. *Metal–Organic Frameworks: Applications from Catalysis to Gas Storage*; John Wiley & Sons: Weinheim, 2011. Batten, S. R.; Neville, S. M.; Turner, D. R. *Coordination Polymers: Design, Analysis and Application*; Royal Society of Chemistry: Cambridge, 2009.
- (3) Clearfield, A. Flexible MOFs under stress: pressure and temperature. *Dalton Trans.* **2016**, *45*, 4100–4112. Schneemann, A.; Bon, V.; Schwedler, I.; Senkowska, I.; Kaskel, S.; Fischer, R. A. Flexible metal–organic frameworks. *Chem. Soc. Rev.* **2014**, *43*, 6062–6096.

Wang, Z.; Cohen, S. M. Modulating Metal–Organic Frameworks To Breathe: A Postsynthetic Covalent Modification Approach. *J. Am. Chem. Soc.* **2009**, *131*, 16675–16677. Chang, Z.; Yang, D.-H.; Xu, J.; Hu, T.-L.; Bu, X.-H. Flexible Metal–Organic Frameworks: Recent Advances and Potential Applications. *Adv. Mater.* **2015**, *27*, 5432–5441.

(4) Llewellyn, P. L.; Horcajada, P.; Maurin, G.; Devic, T.; Rosenbach, N.; Bourrelly, S.; Serre, C.; Vincent, D.; Loera-Serna, L.; Filinchuk, Y.; Férey, G. Complex Adsorption of Short Linear Alkanes in the Flexible Metal–Organic–Framework MIL-53(Fe). *J. Am. Chem. Soc.* **2009**, *131*, 13002–13008. Fletcher, A. J.; Thomas, K. M.; Rosseinsky, M. J. Flexibility in metal–organic framework materials: Impact on sorption properties. *J. Solid State Chem.* **2005**, *178*, 2491–2510. Hawes, C. S.; Hamilton, S. E.; Hicks, J.; Knowles, G. P.; Chaffee, A. L.; Turner, D. R.; Batten, S. R. Coordination Chemistry and Structural Dynamics of a Long and Flexible Piperazine-Derived Ligand. *Inorg. Chem.* **2016**, *55*, 6692–6702. Haraguchi, T.; Otsubo, K.; Sakata, O.; Fujiwara, A.; Kitagawa, H. Remarkable Lattice Shrinkage in Highly Oriented Crystalline Three-Dimensional Metal–Organic Framework Thin Films. *Inorg. Chem.* **2015**, *54*, 11593–11595.

(5) Krause, S.; Bon, V.; Senkowska, I.; Stoeck, U.; Wallacher, D.; Többsens, D. M.; Zander, S.; Pillai, R. S.; Maurin, G.; Coudert, F.-X.; Kaskel, S. A pressure-amplifying framework material with negative gas adsorption transitions. *Nature* **2016**, *532*, 348–352.

(6) Manna, B.; Chaudhari, A. K.; Joarder, B.; Karmakar, A.; Ghosh, S. K. Dynamic structural behavior and anion-responsive tunable luminescence of a flexible cationic metal–organic framework. *Angew. Chem., Int. Ed.* **2013**, *52*, 998–1002.

(7) Deria, P.; Gómez-Gualdrón, D. A.; Bury, W.; Schaefer, H. T.; Wang, T. C.; Thallapally, P. K.; Sarjeant, A. A.; Snurr, R. Q.; Hupp, J. T.; Farha, O. K. Ultraporos, Water Stable, and Breathing Zirconium-Based Metal–Organic Frameworks with ftw Topology. *J. Am. Chem. Soc.* **2015**, *137*, 13183–13190. Haigis, V.; Coudert, F.-X.; Vuilleumier, R.; Boutin, A.; Fuchs, A. H. Hydrothermal Breakdown of Flexible Metal–Organic Frameworks: A Study by First-Principles Molecular Dynamics. *J. Phys. Chem. Lett.* **2015**, *6*, 4365–4370. Hawes, C. S.; Chilton, N. F.; Moubaraki, B.; Knowles, G. P.; Chaffee, A. L.; Murray, K. S.; Batten, S. R.; Turner, D. R. Coordination polymers from a highly flexible alkyldiamine-derived ligand: structure, magnetism and gas adsorption studies. *Dalton Trans.* **2015**, *44*, 17494–17507.

(8) Kitagawa, S.; Uemura, K. Dynamic porous properties of coordination polymers inspired by hydrogen bonds. *Chem. Soc. Rev.* **2005**, *34*, 109–119. Maji, T. K.; Matsuda, R.; Kitagawa, S. A flexible interpenetrating coordination framework with a bimodal porous functionality. *Nat. Mater.* **2007**, *6*, 142–148. Haldar, R.; Inukai, M.; Horike, S.; Uemura, K.; Kitagawa, S.; Maji, T. K.  $^{113}\text{Cd}$  Nuclear Magnetic Resonance as a Probe of Structural Dynamics in a Flexible Porous Framework Showing Selective  $\text{O}_2/\text{N}_2$  and  $\text{CO}_2/\text{N}_2$  Adsorption. *Inorg. Chem.* **2016**, *55*, 4166–4172.

(9) Duke, R. M.; Veale, E. B.; Pfeffer, F. M.; Kruger, P. E.; Gunnlaugsson, T. Colorimetric and fluorescent anion sensors: an overview of recent developments in the use of 1,8-naphthalimide-based chemosensors. *Chem. Soc. Rev.* **2010**, *39*, 3936–3953. Shelton, A. H.; Sazanovich, I. V.; Weinstein, J. A.; Ward, M. D. Controllable three-component luminescence from a 1,8-naphthalimide/Eu(III) complex: white light emission from a single molecule. *Chem. Commun.* **2012**, *48*, 2749–2751. Izawa, H.; Nishino, S.; Sumita, M.; Akamatsu, M.; Morihashi, K.; Ifuku, S.; Morimoto, M.; Saimoto, H. A novel 1,8-naphthalimide derivative with an open space for an anion: unique fluorescence behaviour depending on the binding anion’s electrophilic properties. *Chem. Commun.* **2015**, *51*, 8596–8599.

(10) Stewart, W. W. Lucifer dyes—highly fluorescent dyes for biological tracing. *Nature* **1981**, *292*, 17–21. de Silva, A. P.; Gunaratne, H. Q. N.; Habib-Jiwan, J.-L.; McCoy, C. P.; Rice, T. E.; Soumillion, J.-P. New Fluorescent Model Compounds for the Study of Photo-induced Electron Transfer: The Influence of a Molecular Electric Field in the Excited State. *Angew. Chem., Int. Ed. Engl.* **1995**, *34*, 1728–1731. Veale, E. B.; Frimannsson, D. O.; Lawler, M.; Gunnlaugsson, T. 4-Amino-1,8-naphthalimide-Based Tröger’s Bases As High Affinity DNA

Targeting Fluorescent Supramolecular Scaffolds. *Org. Lett.* **2009**, *11*, 4040–4043. Banerjee, S.; Kitchen, J. A.; Gunnlaugsson, T.; Kelly, J. M. The effect of the 4-amino functionality on the photophysical and DNA binding properties of alkyl-pyridinium derived 1,8-naphthalimides. *Org. Biomol. Chem.* **2013**, *11*, 5642–5655.

(11) Banerjee, S.; Veale, E. B.; Phelan, C. M.; Murphy, S. A.; Tocci, G. M.; Gillespie, L. J.; Frimannsson, D. O.; Kelly, J. M.; Gunnlaugsson, T. Recent advances in the development of 1,8-naphthalimide based DNA targeting binders, anticancer and fluorescent cellular imaging agents. *Chem. Soc. Rev.* **2013**, *42*, 1601–1618. Xu, Z.; Baek, K.-H.; Kim, H. N.; Cui, J.; Qian, X.; Spring, D. R.; Shin, I.; Yoon, J. Zn<sup>2+</sup>-Triggered Amide Tautomerization Produces a Highly Zn<sup>2+</sup>-Selective, Cell-Permeable, and Ratiometric Fluorescent Sensor. *J. Am. Chem. Soc.* **2010**, *132*, 601–610. Lee, M. H.; Han, J. H.; Kwon, P.-S.; Bhuniya, S.; Kim, J. Y.; Sessler, J. L.; Kang, C.; Kim, J. S. Hepatocyte-Targeting Single Galactose-Appended Naphthalimide: A Tool for Intracellular Thiol Imaging in Vivo. *J. Am. Chem. Soc.* **2012**, *134*, 1316–1322. Dai, Z.-R.; Ge, G.-B.; Feng, L.; Ning, J.; Hu, L.-H.; Jin, Q.; Wang, D.-D.; Lv, X.; Dou, T.-Y.; Cui, J.-N.; Yang, L. A Highly Selective Ratiometric Two-Photon Fluorescent Probe for Human Cytochrome P450 1A. *J. Am. Chem. Soc.* **2015**, *137*, 14488–14495.

(12) Ogi, S.; Stepanenko, V.; Thein, J.; Würthner, F. Impact of Alkyl Spacer Length on Aggregation Pathways in Kinetically Controlled Supramolecular Polymerization. *J. Am. Chem. Soc.* **2016**, *138*, 670–678. Reger, D. L.; Leitner, A.; Smith, M. D. Homochiral, Helical Coordination Complexes of Lanthanides(III) and Mixed-Metal Lanthanides(III): Impact of the 1,8-Naphthalimide Supramolecular Tecton on Structure, Magnetic Properties, and Luminescence. *Cryst. Growth Des.* **2015**, *15*, 5637–5644. Veale, E. B.; Gunnlaugsson, T. Synthesis, Photophysical, and DNA Binding Studies of Fluorescent Tröger's Base Derived 4-Amino-1,8-naphthalimide Supramolecular Clefs. *J. Org. Chem.* **2010**, *75*, 5513–5525. Ryan, G. J.; Elmes, R. B. P.; Erby, M.; Poynton, F. E.; Williams, D. C.; Quinn, S. J.; Gunnlaugsson, T. Unexpected DNA binding properties with correlated downstream biological applications in mono vs. bis-1,8-naphthalimide Ru(II)-polypyridyl conjugates. *Dalton Trans.* **2015**, *44*, 16332–16344. Banerjee, S.; Bright, S. A.; Smith, J. A.; Burgeat, J.; Martinez-Calvo, M.; Williams, D. C.; Kelly, J. M.; Gunnlaugsson, T. A Supramolecular Approach to Enantioselective DNA Recognition using Enantiomerically Resolved Cationic 4-Amino-1,8-Naphthalimide based Tröger's Bases. *J. Org. Chem.* **2014**, *79*, 9272–9283.

(13) Mukherjee, S.; Thilagar, P. Insights into the AIEE of 1,8-Naphthalimides (NPIs): Inverse Effects of Intermolecular Interactions in Solution and Aggregates. *Chem. - Eur. J.* **2014**, *20*, 8012–8023.

(14) Mukherjee, S.; Thilagar, P. Molecular flexibility tuned emission in "Y" shaped naphthalimides: Hg(II) detection and aggregation-induced emission enhancement (AIEE). *Chem. Commun.* **2013**, *49*, 7292–7294. Biczók, L.; Valat, P.; Wintgens, V. Effect of molecular structure and hydrogen bonding on the fluorescence of hydroxy-substituted naphthalimides. *Phys. Chem. Chem. Phys.* **1999**, *1*, 4759–4766. Magalhães, J. L.; Pereira, R. V.; Triboni, E. R.; Filho, P. B.; Gehlen, M. H.; Nart, F. C. Solvent effect on the photophysical properties of 4-phenoxy-N-methyl-1,8-naphthalimide. *J. Photochem. Photobiol., A* **2006**, *183*, 165–170.

(15) Kitchen, J. A.; Martinho, P. N.; Morgan, G. G.; Gunnlaugsson, T. Synthesis, crystal structure and EPR spectroscopic analysis of novel copper complexes formed from N-pyridyl-4-nitro-1,8-naphthalimide ligands. *Dalton Trans.* **2014**, *43*, 6468–6479. Reger, D. L.; Leitner, A. P.; Smith, M. D. Supramolecular Metal–Organic Frameworks of s- and f-Block Metals: Impact of 1,8-Naphthalimide Functional Group. *Cryst. Growth Des.* **2016**, *16*, 527–536. Reger, D. L.; Semeniuc, R. F.; Elgin, J. D.; Rassolov, V.; Smith, M. D. 1,8-Naphthalimide Synthon in Silver Coordination Chemistry: Control of Supramolecular Arrangement. *Cryst. Growth Des.* **2006**, *6*, 2758–2768. Reger, D. L.; Debreczeni, A.; Smith, M. D. Zinc Paddlewheel Dimers Containing a Strong  $\pi\cdots\pi$  Stacking Supramolecular Synthon: Designed Single-Crystal to Single-Crystal Phase Changes and Gas/Solid Guest Exchange. *Inorg. Chem.* **2011**, *50*, 11754–11764.

(16) Han, L.; Qin, L.; Xu, L.; Zhou, Y.; Sun, J.; Zou, X. A novel photochromic calcium-based metal–organic framework derived from a naphthalene diimide chromophore. *Chem. Commun.* **2013**, *49*, 406–408. Leong, C. F.; Faust, T. B.; Turner, P.; Usov, P. M.; Kepert, C. J.; Babarao, R.; Thornton, A. W.; D'Alessandro, D. M. Enhancing selective CO<sub>2</sub> adsorption via chemical reduction of a redox-active metal–organic framework. *Dalton Trans.* **2013**, *42*, 9831–9839. Wade, C. R.; Li, M.; Dincă, M. Facile Deposition of Multicolored Electrochromic Metal–Organic Framework Thin Films. *Angew. Chem., Int. Ed.* **2013**, *52*, 13377–13381. McCormick, L. J.; Turner, D. R. Inclined 1D→2D polycatenation of chiral chains with large  $\pi$ -surfaces. *CrystEngComm* **2013**, *15*, 8234–8236.

(17) Genuis, E. D.; Kelly, J. A.; Patel, M.; McDonald, R.; Ferguson, M. J.; Greidanus-Strom, G. Coordination Polymers from the Self-Assembly of Silver(I) Salts and Two Nonlinear Aliphatic Dinitrile Ligands, cis-1,3-Cyclopentanedicarbonitrile and cis-1,3-Bis-(cyanomethyl)cyclopentane: Synthesis, Structures, and Photoluminescent Properties. *Inorg. Chem.* **2008**, *47*, 6184–6194. Min, K.-S.; Suh, M. P. Silver(I)–Polynitrile Network Solids for Anion Exchange: Anion-Induced Transformation of Supramolecular Structure in the Crystalline State. *J. Am. Chem. Soc.* **2000**, *122*, 6834–6840. Beeching, L. J.; Hawes, C. S.; Turner, D. R.; Batten, S. R. The influence of anion, ligand geometry and stoichiometry on the structure and dimensionality of a series of AgI-bis(cyanobenzyl)piperazine coordination polymers. *CrystEngComm* **2014**, *16*, 6459–6468.

(18) Drew, M. G. B.; Harding, C. J.; McKee, V.; Morgan, G. G.; Nelson, J. Geometric control of manganese redox state. *J. Chem. Soc., Chem. Commun.* **1995**, 1035–1038.

(19) Chen, K.-J.; Madden, D. G.; Pham, T.; Forrest, K. A.; Kumar, A.; Yang, Q.-Y.; Xue, W.; Space, B.; Perry, J. J. P., IV; Zhang, J.-P.; Chen, X.-M.; Zaworotko, M. J. Tuning Pore Size in Square-Lattice Coordination Networks for Size-Selective Sieving of CO<sub>2</sub>. *Angew. Chem., Int. Ed.* **2016**, *55*, 10268–10272. Pillai, R. S.; Benoit, V.; Orsi, A.; Llewellyn, P. L.; Wright, P. A.; Maurin, G. Highly Selective CO<sub>2</sub> Capture by Small Pore Scandium-Based Metal–Organic Frameworks. *J. Phys. Chem. C* **2015**, *119*, 23592–23598. Scott, H. S.; Ogiwara, N.; Chen, K.-J.; Madden, D. G.; Pham, T.; Forrest, K.; Space, B.; Horike, S.; Perry, J. J. P., IV; Kitagawa, S.; Zaworotko, M. J. Crystal engineering of a family of hybrid ultramicroporous materials based upon interpenetration and dichromate linkers. *Chem. Sci.* **2016**, *7*, 5470–5476. Ziaee, A.; Chovan, D.; Lusi, M.; Perry, J. J. P., IV; Zaworotko, M. J.; Tofail, S. A. M. Theoretical Optimization of Pore Size and Chemistry in SIFSIX-3-M Hybrid Ultramicroporous Materials. *Cryst. Growth Des.* **2016**, *16*, 3890–3897. McCormick, L. J.; Duyker, S. G.; Thornton, A. W.; Hawes, C. S.; Hill, M. R.; Peterson, V. K.; Batten, S. R.; Turner, D. R. Ultramicroporous MOF with High Concentration of Vacant Cu<sup>II</sup> Sites. *Chem. Mater.* **2014**, *26*, 4640–4646.

(20) Brouwer, A. M. Standards for photoluminescence quantum yield measurements in solution (IUPAC Technical Report). *Pure Appl. Chem.* **2011**, *83*, 2213–2228.

(21) Mukherjee, S.; Thilagar, P. Fine-tuning solid-state luminescence in NPIs (1,8-naphthalimides): impact of the molecular environment and cumulative interactions. *Phys. Chem. Chem. Phys.* **2014**, *16*, 20866–20877.

(22) Feitelson, J. On the Mechanism of Fluorescence Quenching. Tyrosine and Similar Compounds. *J. Phys. Chem.* **1964**, *68*, 391–397. Ricci, R. W.; Nesta, J. M. Inter- and intramolecular quenching of indole fluorescence by carbonyl compounds. *J. Phys. Chem.* **1976**, *80*, 974–980.

(23) Veale, E. B.; Kitchen, J. A.; Gunnlaugsson, T. Fluorescent tren-based 4-amino-1,8-naphthalimide sensor for Cu(II) based on the use of the (fluorophore-spacer-receptor) Photoinduced Electron Transfer (PET) principle. *Supramol. Chem.* **2013**, *25*, 101–108.

(24) Janiak, C. A critical account on  $\pi$ - $\pi$  stacking in metal complexes with aromatic nitrogen-containing ligands. *J. Chem. Soc., Dalton Trans.* **2000**, 3885–3896. Klosterman, J. K.; Yamauchi, Y.; Fujita, M. Engineering discrete stacks of aromatic molecules. *Chem. Soc. Rev.* **2009**, *38*, 1714–1725.

(25) Bruker APEX-3; Bruker-AXS Inc.: Madison, WI, 2016.

- (26) SADABS; Bruker-AXS Inc.: Madison, WI, 2016.
- (27) Sheldrick, G. M. SHELXT – Integrated space-group and crystal-structure determination. *Acta Crystallogr., Sect. A: Found. Adv.* **2015**, *71*, 3–8.
- (28) Sheldrick, G. M. Crystal structure refinement with SHELXL. *Acta Crystallogr., Sect. C: Struct. Chem.* **2015**, *71*, 3–8.
- (29) Dolomanov, O. V.; Bourhis, L. J.; Gildea, R. J.; Howard, J. A. K.; Puschmann, H. OLEX2: a complete structure solution, refinement and analysis program. *J. Appl. Crystallogr.* **2009**, *42*, 339–341.
- (30) Spek, A. L. PLATON SQUEEZE: a tool for the calculation of the disordered solvent contribution to the calculated structure factors. *Acta Crystallogr., Sect. C: Struct. Chem.* **2015**, *71*, 9–18.